# RSC Advances

ROYAL SOCIETY OF CHEMISTRY

www.rsc.org/advances
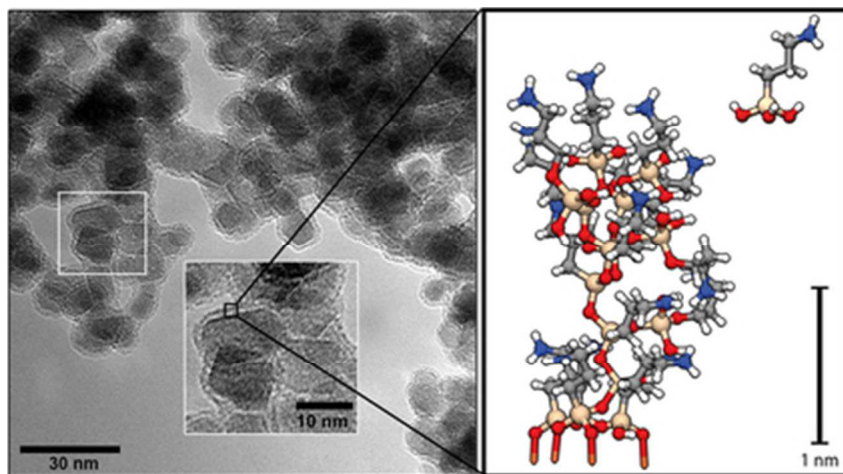
35x20mm (300 x 300 DPI)

# Journal Name

## ARTICLE

# Morphology and properties of silica-based coatings with different functionalities for Fe$_3$O$_4$, ZnO and Al$_2$O$_3$ nanoparticles

D. Liu[a], A. M. Pourrahimi[a], L. K. H. Pallon[a], R. L. Andersson[a], M. S. Hedenqvist[a],
U. W. Gedde[a], R. T. Olsson[a],*

A facile single-step method for obtaining 2–3 nm thick silsesquioxane coatings on metal oxide nanoparticles using different carbon-functional silane precursors is presented. Iron oxide nanoparticles 8.5 nm in diameter were used as a model to evaluate the possibilities of forming different uniform carbon-functional coatings, ranging from hydrophobic to hydrophilic in character. Electron microscopy showed that all the coated nanoparticles could be described as core-shell nanoparticles with single Fe$_3$O$_4$ cores and carbon-functional silsesquioxane shells, without any core-free silicone oxide phase. Steric factors strongly influenced the deposited silicon oxide precursors with octyl-, methyl- or aminopropyl functionalities, resulting in coating densities ranging from 260 to 560 kg/m$^3$. The methyl-functional coatings required several layers of silsesquioxane, 3–4, to build up the 2 nm structures, whereas only 1-2 layers were required for silsesquioxane with octyl groups. Pure silica coatings from tetraethoxysilanes were however considerably thicker due to the absence of steric hindrance during deposition, allowing the formation of 5–7 nm coatings of ca. 10 layers. The coating method developed for the iron oxide nanoparticles was generic and successfully transferred and up–scaled 30 and 325 times (by volume) to be applicable to 25 nm ZnO and 45 nm Al$_2$O$_3$ nanoparticles.

## 1. Introduction

Extruded high-voltage direct current cables insulated with crosslinked polyethylene are currently commercially available up to 525 kV for both submarine and underground applications. [1, 2, 3] To meet the forecast energy/power demands, a targeted maximum voltage for the cables in the year 2030 is 1 MV to reduce energy losses.[4] This requires a significant decrease in the electrical conductivity of the insulating PE material.[1] Two different strategies are currently emerging. One is to further refine the PE by reducing the concentration of mobile ionic and polar species originating from the vulcanization and polymerization.[1] The second strategy is to include uniformly dispersed metal oxide nanoparticles, e.g. ZnO, MgO and Al$_2$O$_3$, at a low concentration (< 3 wt.%) in the polymer. This strategy appears promising and early experiments indicate a ten-fold decrease in the electrical conductivity as a result of the reduced mobility of charges within the large polymer interphase surrounding the particles.[5] The achievement of a large polymer interphase is however one of the greatest challenges with polyethylene, since inorganic particles are incompatible with the polymer. Solid methods to vary particle interfaces on a large scale are therefore important not only for good dispersions from a mechanistic viewpoint but also because they are likely to have a great impact on the insulation capacity of the next generation of high-voltage cable insulations currently under development.

Methods to modify nanoparticles with electrostatically adsorbed coatings have been presented,[6] but the robustness of the coatings is limited when the particles are extruded with the PE under high shear forces and high temperatures. Covalently cross-linked silsesquioxane coatings with integrated carbon functionalities may improve the compatibility with PE, and present an intact chemical/physical protection to the inorganic cores during the melt processing (extrusion).[7, 8, 9] One benefit of using the silsesquioxne coatings is that they are derived from commercial and inexpensive silane molecules. Another advantage is that the coating formation relies on water/alcohol-based condensation chemistry, which can potentially easily be up–scaled. However, carbon-functional silsesquioxane coatings of substantial thicknesses are rarely reported in comparison to silica coatings.

Different methods have been reported to generate thick silsequioxane coatings on nanoparticles: **1.** Zhang et al. [10] used

microemulsions to obtain uniform 20 nm thick amino–functional coatings from methoxy-functional silanes. The uniformity of the coating thickness was the major advantage of this method,[11] whereas the separation processes required to remove the excess surfactant, the limited yield of material per reaction volume, and the use of a non-aqueous reaction medium are draw-backs. **2.** Goyal and Huang et al.[12, 13] used anhydrous solvents as reaction media to prevent silicone oxide condensation from occurring apart from on the surface of the nanoparticles. However, these reactions require the complete elimination of all the particle-associated water via a solvent exchange method, which is difficult to verify for particles having an extremely large surface area. **3.** The third method is based on the Liz-Marzán version of the Stöber method, in which particle coatings are formed in alcohol/water mixtures by condensation and further deposition on the particle surfaces'.[14, 15, 16] To prevent the aggregation of nanoparticles during the coating reactions, the use of different surfactants (acting as a template for silica growth) has been reported as a prior coating step.[14, 17, 18, 19] The surfactant also facilitates deposition of the coating on very small particles (<20 nm) with high surface curvature.[20, 21] However, the additional coating step requires a very long reaction time (up to 24 h) and the removal of excess surfactant requires extensive washing [17, 22] and there is a risk of core-free micro-emulsion with excess surfactant. There is thus a need to develop industrially relevant coating methods applicable to very small nanoparticles (< 20 nm) that do not require the use of surfactants.

This work presents for the first time a comparison of the possibilities to obtain relatively thick silsequioxane coatings without any intermediate surfactant coating steps or anhydrous solvent-based reactions. We report the coating of 8 nm $Fe_3O_4$ nanoparticles with 2–7 nm silicon oxide coatings (silsesquioxane and silica). Silsesquioxane coatings with different functionalities aminopropyl-, methyl- and octyl-functional silicon oxide were studied, in addition to the silica coating used as comparison. The reactions conditions developed were generic and successfully up-scaled to both 25 nm ZnO and 45 nm $Al_2O_3$ nanoparticles. The mechanisms for the growth of the coatings on the nanoparticle cores were analysed modelling the steric configuration of the precursor molecules, and the results are discussed in relation to the obtained coatings that were formed under identical conditions.

## 2. Experimental section

### 2.1 Chemicals

Iron (II) chloride tetrahydrate ($FeCl_2 \cdot 4H_2O$, $\geq$ 99%), iron (III) chloride hexahydrate ($FeCl_3 \cdot 6H_2O$, $\geq$ 98%) and ammonium hydroxide (25%) were used to prepare the $Fe_3O_4$ nanoparticles. Zinc acetate dehydrate ($Zn(CH_3COO)_2 \cdot 2H_2O$) and sodium hydroxide (NaOH) were used to prepare the ZnO nanoparticles. (3-aminopropyl) triethoxysilane (APTES, $\geq$ 98%; $\rho$ = 946 kg/m$^3$, $M$ =221.4 Da), methyltrimethoxysilane (MTMS, $\geq$ 95%, $\rho$ = 955 kg/m$^3$, $M$ =136.2 Da), octyltriethoxysilane (OTES, $\geq$

98%, $\rho$ = 880 kg/m$^3$, $M$ =276.5 g/mol)) and tetraethoxysilane (TEOS, $\geq$ 98%, $\rho$=933 kgm$^{-3}$, $M$=208.3 Da) were used to coat metal oxide particles. The chemicals were purchased from Sigma-Aldrich and used without further purification. The reaction media were high-resistivity MilliQ water ("Type 1", following ISO 3696 and ASTM D1193–91, defined as 18.2 MOhm.cm at 25°C) and isopropanol ($\geq$ 99.5%, Sigma-Aldrich). Aluminium oxide nanoparticles of 99.5% purity (Nanodur, CAS: 1344–28–1), consisting of almost spherical particles with an average diameter of 45 nm (70 wt% δ-phase and 30 wt% γ-phase), were purchased from Nanophase Inc. USA. Ethanol ($\geq$ 96%, VWR) was used to wash the coated nanoparticles.

### 2.2 Synthesis of silsesquioxanes-coated iron oxide nanoparticles

The $Fe_3O_4$ nanoparticles were synthesized by a rapid mixing technique according to Olsson et al.[23, 24, 25] The synthesis was carried out as separate samples, "shots", from two adjacent syringes, each sample giving a total of 11.5 mg iron oxide in the form of $Fe_3O_4$ nanoparticles with a specific surface area of 141 m$^2$/g.[23] Prior to the following coating experiments, the prepared nanoparticles (also including 2.3) were ultrasonically cleaned from counter ions by immersion of the particle suspensions in a Bandelin RK100H bath (output of 320 W).[26]

The iron oxide nanoparticles were maintained wet after removal of residual reactants and dispersed in 0.68 mL $H_2O$ to which 3.14 mL 2-propanol was added. 0.085 mL (2.13 vol.%) ammonia (25 vol.%) was added to the $Fe_3O_4$ suspension, followed by vigorous shaking for 5 min on a Vortex Shaker. The $Fe_3O_4$ particles were coated by polymerizing the silsesquioxane precursors to the particle surfaces using a modified Stöber method.[16] 90 μL silane was added to initiate the coating reaction. The amount of silane was equivalent to 0.056 mL/m$^2$. The reaction was performed at 20 °C for 3 h. The silsesquioxane-coated $Fe_3O_4$ nanoparticles were re-dispersed in ethanol after centrifugation and washing thrice with ethanol. The silica coating was applied identically and the effect of incubation time on the TEOS coating was studied by interrupting the shell growth after 0.5, 1 and 3 h by adding 0.2 mL of the reaction suspension to 1.5 mL water, followed by centrifugation and washing to remove unreacted TEOS.

### 2.3 Preparation of OTES-coated ZnO nanoparticles

ZnO nanoparticles (25 nm prisms) were prepared by an aqueous precipitation method according to Pourrahimi et al.[26] A 0.2 M zinc acetate aqueous solution was mixed with a 0.5 M NaOH aqueous solution under vigorous stirring at 60 °C for 1 h. The resulting ZnO particles were washed thrice with water before surface modification. 0.3 g ZnO particles with a specific surface area of 34 m$^2$/g (BET measurement) were coated in a mixed solvent of 20.4 mL water and 94.2 mL 2–propanol. Then, 2.55 mL ammonia (25 vol.%) was added to the ZnO suspension, and the suspension was stirred for 5 min. Finally, 2.7 mL octyltriethoxysilane (OTES) was added to the suspension and allowed to react for 3 h at 20 °C, which was equivalent to a silane amount of 0.21 mL/m$^2$. The coated particles were washed and dried at 80 °C overnight.

### 2.4 Preparation of OTES-coated aluminium oxide nanoparticles

3.84 g of $Al_2O_3$ particles with a specific surface area of 36 $m^2$/g (BET measurement) were dispersed in a mixture of 163.2 mL water and 753.6 mL 2-propanol. 20.4 mL ammonia (25 vol.%) was added to the $Al_2O_3$ suspension and mechanically stirred for 5 min. 21.6 mL OTES was then added and allowed to react for 24 h at 20 °C, which was equivalent to a silane amount of 0.17 mL/$m^2$. The coated particles were washed and dried at 80 °C overnight.

### 2.5 Etching procedure for determination of the mass and density of the silsesquioxane and silica coatings

The mass of the coatings on the core-shell particles were obtained by weighing coated iron oxide samples before and after removal of the coatings by etching. The coated particles were first dried at 50 °C in a vacuum oven overnight. Each dry sample (mass = $w_1$) was weighted on an analytical balance (Mettler-Toledo, Switzerland), and the particles were then re-dispersed in 10 vol.% concentrated NaOH solution, and treated with a micro-tip probe fitted to an ultrasonicator: Sonics VibraCell 750 W, used at 27 % of maximum power for 90 s (15 s × 6) at 50 °C. The particles were concentrated by applying a NdFeB magnet, the supernatants were decanted off, and the procedure was repeated twice. The particles were finally washed with water and dried in a vacuum oven at 50 °C overnight. The mass of each sample after etching ($w_2$) was then determined. The mass fraction of the coating was obtained as ($w_1$-$w_2$)/$w_2$. Three measurements were conducted for each sample.

### 2.6 Characterization

Transmission electron micrographs were taken with a Hitachi HT7700 microscope at 100 kV. Samples were deposited on carbon-coated 400 mesh copper grids (Ted Pella, Inc., USA) from ultrasonicated ethanol suspensions of the particles. The size of nanoparticles and the thickness of the coatings were determined using the software Image J (National Institutes of Health, USA). Dynamic light scattering experiments were conducted with a Malvern Zetasizer Nano ZS (Malvern, UK). The measurements were made with a 633 nm He/Ne laser at a temperature of 25 ℃ on aqueous suspensions of the particles. Attenuated Total Reflection Infrared spectra were recorded on a Perkin-Elmer IR Spectrometer 2000 equipped with a single reflection ATR accessory (Golden Gate) from Graseby Specac, UK. A Mettler-Toledo SDTA/TGA905 thermo-balance was used to obtain the mass of the nanoparticle samples before and after the surface modification. The samples kept in 70 μL aluminium oxide crucibles were heated from 40 to 800 °C at a rate of 10 °C/min in nitrogen. All the samples were dried in a vacuum oven at 50 °C overnight before the thermogravimetry and IR spectroscopy. The EDS (Energy Dispersive X-Ray Spectroscopy) spectra were acquired on a Hitachi S-4800 SEM, equipped with an Oxford Instruments X-Max$^N$ 80 EDS.

### 2.7 Molecular modelling

The silsesquioxane shells were built using the UCSF Chimera software 1.10 (Resource for Biocomputing, Visualization, and Informatics, San Francisco, USA). All atomic and bond features were taken directly from the software. The bond angle in the Fe-O-Si sequence was considered to be that for trigonal oxygen (120°), which is close to the 116° angle reported in Nontronite (Avogadro software 1.1.1, open-source molecular builder and visualization tool, avogadro.openmolecules.net).

## 3 Results and discussion

### 3.1 Preparation and coating of $Fe_3O_4$ nanoparticles

Fig. 1a shows transmission electron micrographs and size-histograms of the precipitated $Fe_3O_4$ nanoparticles; the average particle size was 8.5 nm and the calculated surface area was 141 $m^2$/g. The particles were prepared as several separate and identical 11.5 mg batches by rapid mixing (8 m/s) of a 0.22 M iron chloride solution with a 4 M ammonia solution, with approximately 7.16 × $10^{15}$ particles in each tube used for the surface modification reactions.[23, 24, 25] A clean spinel oxide magnetite phase[24] was consistent with the previously taken electron diffraction patterns (SAED).[23, 25] The particle surfaces were cleaned from counter-ions by ultrasonication[26], which resulted in stable colloidal suspensions in water with a zeta potential of +34 mV at pH 5.5.
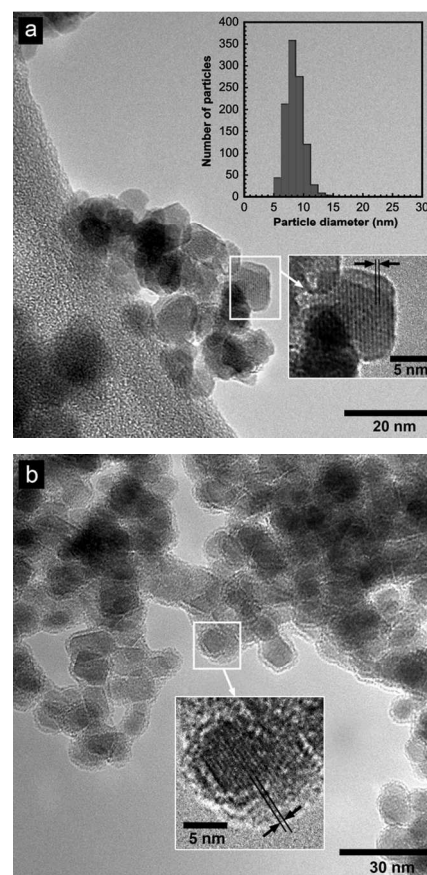
**Fig. 1.** (a). TEM of $Fe_3O_4$ nanoparticles with a histogram showing the particle size distribution (inset graph, top) and interplanar lattice fringe distance measured to 0.49 nm (insert micrograph, bottom), corresponding to (111) planes of the $Fe_3O_4$ crystals with a cubic inverse spinel structure. (b). TEM of the same nanoparticles after coating with a 1.5-2.5 nm APTES coating

Fig. 1b shows a micrograph of the same $Fe_3O_4$ nanoparticles with a 1.5–2.5 nm thick and uniform APTES silsesquioxane coating covering the individual particles. The TEM image confirmed that the nanoparticles retained their original morphology (Fig. 1a) and the crystal lattice of iron oxide could be observed at higher magnification after the coating process. The (111) planes had an interplanar distance of 0.49 nm that was in accordance with data reported by Lu et al.[27], and a crystallographic plane reflection at 18.3° scattering angle (2θ) according to JCPDS reference pattern 00–001-1053. In order to verify that the solitary inorganic cores had been coated, dynamic light scattering measurements after solvent exchange to water were used. The APTES-coated particles showed accumulated peaks at 29 and 78 nm with the smallest particles at ca. 10 nm (zeta potential ≈ +27 mV at pH 5.5), whereas the uncoated nanoparticles showed accumulated peaks at 58 and 110 nm with the smallest particles at ca. 30 nm at pH 5.5 (supplementary info; Fig. S1). These values were also smaller than those for the aggregates revealed on the TEM grids (Fig. 2). The combination of the ultrasonic particle cleaning (resulting in colloidal stability), with the use of 2–propanol with a relative permittivity ε of 18.3, was therefore suggested to

have enabled a coating growth rate that allowed formation and deposition of uniform coatings.

**3.2 Evaluation of reaction conditions for different silanes**

The reaction conditions were evaluated for the silanes with methyl and octyl groups attached to the silicon atom. Fig. 2 shows that coatings with single cores could be obtained for both MTMS and OTES (Figs. 2b and c) under the same reaction conditions as those used for APTES (Fig. 2a). All the silsesquioxane-modified nanoparticle samples showed solitary coated nanoparticles with a core-shell structure and coatings in the thickness range from 1.5 to 2.5 nm, although aggregation is visible in Figs. 2a - c. This aggregation was inevitable, as the particles were deposited and dried on the hydrophobic carbon surface of the TEM grids. For comparison, Fig. 2d shows the iron oxide nanoparticles coated under the same conditions with TEOS (yielding silica coatings ($SiO_2$)). The silica-coated particles were inter-condensed in lumps spread over the TEM grid and had grown together at a later stage of the reaction, since individually coated particles could still be discerned in the aggregated clusters (Fig. 2d). Fig. 3 shows micrographs of the TEOS-coated nanoparticles after different reaction times. The coating thickness increased from 1.4 nm after half an hour (Fig. 3a) to 3.0 nm after one hour (Fig. 3b) and 5.5 nm after three hours (Fig. 2d), *i.e.* when the coated particles had merged into inter-condensed aggregates. From the micrographs, it was concluded that inter-condensation of the solitary silica-coated (TEOS) structure began after one hour.
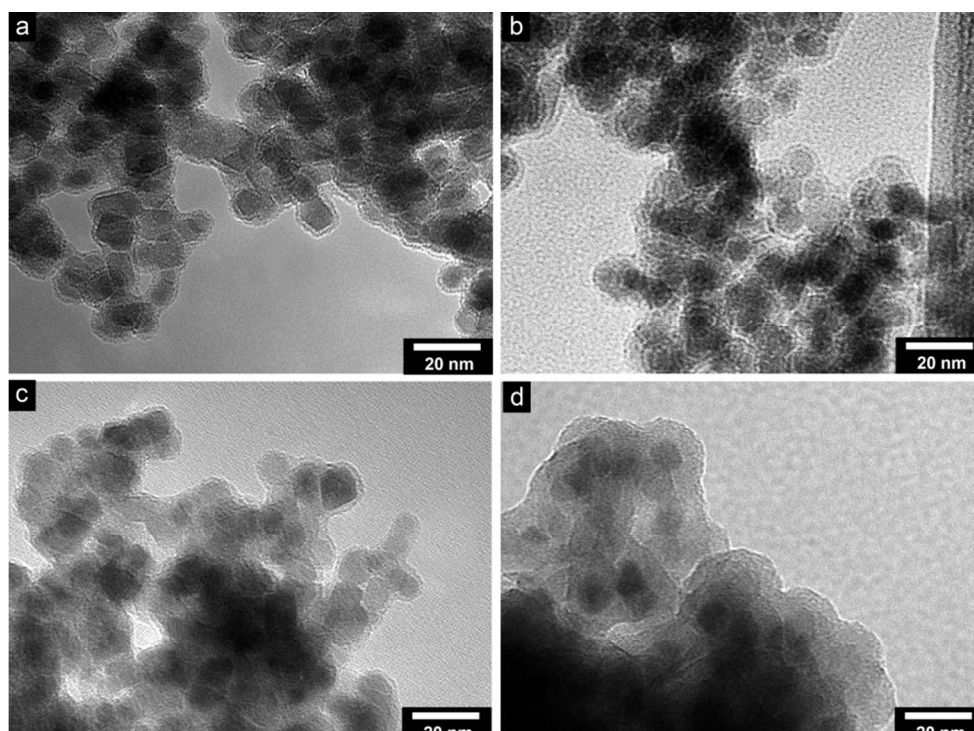


**Fig. 2.** Transmission electron micrographs of silsesquioxane- or silica-coated $Fe_3O_4$ nanoparticles: (a) APTES-coated; *coating thickness* = 1.5–2.5 nm, aver. 2.1 nm (b) MTMS-coated; coating thickness = 1.5-2.5 nm, aver. = 1.8 nm (c) OTES-coated: coating thickness = 1.5–2.5 nm, aver. = 1.7 nm. (d) TEOS-coated; coating thickness = 5-7 nm, aver. = 5.5 nm. Micrographs were taken in high contrast mode setting, allowing clearly visible low-density coatings with dense nanoparticle cores.
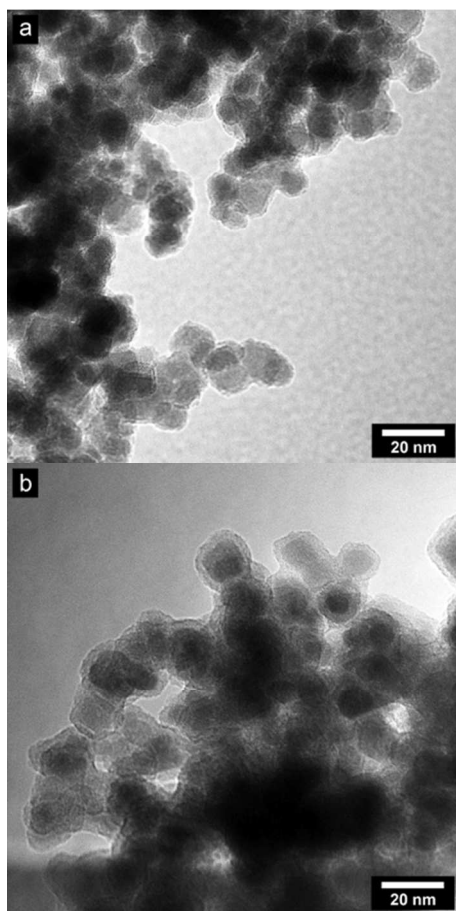
# Journal Name

## ARTICLE



Fig. 3. Transmission electron micrographs of silica-coated $Fe_3O_4$ nanoparticles after different reaction times: (a) 0.5 h, (b) 1 h

The effect of ammonia concentration on the morphology of the coated $Fe_3O_4$ nanoparticles, was examined (Fig. S.I.2) using twice (4.46 vol.%), or half (1.26 vol.%) the reference concentration of ammonia, since the ammonia concentration was previously reported to affect the thickness of silica coatings.[21, 22] A solution of water and isopropanol was used due to the slower rate of condensation of the silanes in alcohols than in water[20, 27]. The variation in ammonia concentration did not affect the thickness of the APTES- and MTMS-coatings. However, no OTES-coating was formed when 1.26 vol.% of ammonia was used and the thickness of the OTES coating did not increase with the ammonia concentration was increased from 2.23 vol.% to 4.46 vol.%. The thickness of the TEOS-coating was very sensitive to the ammonia concentration. A thinner uniform silica coating was formed with a low ammonia concentration, whereas large aggregates were formed with a

high ammonia concentration, which was consistent with the results obtained by Wu et al.[22] and Yang et al.[28]

A four-fold increase in the silane concentration did not affect the coating thickness for the APTES, MTMS and OTES silanes (Fig. S.I.3). This suggested that the growth of thicker silsesquioxane coatings on the particle surface was limited by the presence of carbon-functional groups, because no such thickness limitation was observed with the TEOS-coatings which lacked a carbon functionality. The fact that the reaction time (3 to 12 h) had no effect on the thickness of the carbon-functional coatings further supported this hypothesis.

### 3.3 IR spectroscopy of coated and uncoated nanoparticles

Fig. 4 shows the IR spectra of uncoated and carbon-functional silsesquioxanes-coated $Fe_3O_4$ nanoparticles. All the samples showed broad absorption bands at $3200 - 3500$ cm$^{-1}$ originating from the hydroxyl group on the surface of the particles, uncondensed silanol groups present in the coating shells, and also residual physically and chemically adsorbed water on the surfaces of the nanoparticles.[15] The absorption bands at $990 - 1090$ cm$^{-1}$ were assigned to the asymmetric Si-O-Si stretching vibration, which confirmed the formation of a condensed silicon oxide network structure.[15] This characteristic band was most apparent in the case of the TEOS-coating with a strong peak at 1056 cm$^{-1}$, Fig. 4 (spectrum 1). The absorption of the $-NH_2$ bending/scissoring vibration at 1560 cm$^{-1}$ and of the $-CH$ stretching vibration at 2800–2950 cm$^{-1}$ were characteristics of the APTES-coated particles[15, 29], Fig. 4 (spectrum 2). The MTMS-coating was confirmed by the absorption at 1270 cm$^{-1}$, which was assigned to the Si–CH$_3$ stretching vibration, Fig. 4 (spectrum 3).[15] The clear absorption band at 2800–3000 cm$^{-1}$ from the asymmetric and symmetric -CH stretching vibrations of the methylene and methyl groups (2956 and 2970 cm$^{-1}$) confirmed the presence of the octyl-functionality, Fig. 4 (spectrum 4).

From the repeated scans it was concluded that the relative intensity of the absorption peak associated with a condensed silicon oxide network structure (990-1090 cm$^{-1}$) decreased with increasing size of the carbon functionality. In the OTES coating, the asymmetric Si–O–Si stretching was absent, whereas the shorter carbon-functional units in the APTES- and MTMS-coatings showed absorption at 1006 cm$^{-1}$ and 994 cm$^{-1}$, respectively. This can be compared with the three narrow Si–O–Si peaks associated with the network in the TEOS-coated nanoparticles (spectrum 1), which originated from small non-repulsing silanol groups that could readily condense into a thick densely cross-linked silicon oxide network.[30] Accordingly, the relatively large octyl-functional group (size = 1.42 nm)[31] must have prevented the formation of most of the silicon oxide

bridges. The dominant carbon functionality in the OTES coating was also confirmed by EDS (TEM), showing a relatively weak Si signal (diluted) as compared to iron content, Fig. S4. The Si/Fe ratio was 0.022 compared to 1.8 for the TEOS coating, which was in agreement with the expected contents from the etching experiments (section 3.4).
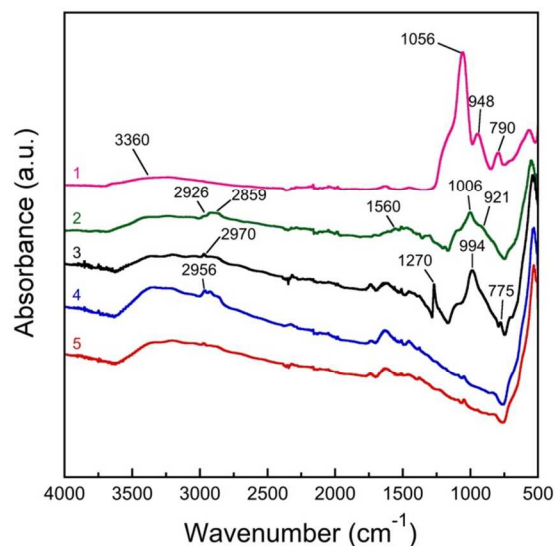


**Fig. 4.** IR spectra of core-shell nanoparticles; (1) TEOS-coated $Fe_3O_4$, (2) APTES-coated $Fe_3O_4$, (3) MTMS-coated $Fe_3O_4$, (4) OTES-coated $Fe_3O_4$, (5) uncoated $Fe_3O_4$. All the samples were dried under vacuum at 50 °C for 24 h prior to characterization.

### 3.4 Determination of the coating mass and density of silsesquioxane/silica shells attached to the nanoparticles by removal of the coatings

Fig. 5 shows the mass loss of the nanoparticles when they were heated from 120 °C to 800 °C in nitrogen. The initial mass loss due to the release of water was observed for all the samples.[32] The amounts of water released at 200 °C were 0.8 % (uncoated), 0.6 % (APTES), 0.6 % (MTMS), 0.9 % (OTES) and 0.4 % (TEOS). The amount of water released at 200 °C was 0.2 wt.% higher for the uncoated nanoparticles than for the MTMS-coated nanoparticles, due to the dry initial state of the hydrophobic MTMS-coating. For the OTES coating, the initial mass loss rate up to 200 °C was the same as that for the uncoated particles; the latter lost 0.8 wt.% due to condensation of surface-located hydroxyl groups (Fig 5, insert graph).

The fractions of silsesquioxane coatings on the nanoparticle cores were estimated from the mass losses between 200 °C and 800 °C (Fig. 5), assuming that the carbon-functional units degraded, dissipated from the particle surfaces and were replaced with a silica ($SiO_2$) network. The APTES coating constituted 16.9 wt.%, the MTMS: 36.3 wt.%, and the OTES 9.7 wt.% of the core-shell particles. The thermogravimetric data are, however, only semi-quantitative, because water must also have dissipated when Si–O–Si bridges formed during the heating to 800 °C.[15, 33] The greater mass loss above 200 °C for the TEOS-coated particles supported this hypothesis (Fig. 5: curve 2) showing that structural reorganization with additional condensation reactions in the silica network shells occurred in the absence of carbon-functional units. This reorganization was previously associated with the formation of a more constrained cross-linked $SiO_2$ network.[32]

In order to obtain a more reliable estimate of the coating fraction, the coatings were removed by NaOH-etching, and the mass loss associated with this procedure was taken as an absolute value for the coating mass. The complete removal of the coatings from the nanoparticles was confirmed by IR spectroscopy. The mass percentages of the APTES, MTMS and OTES coatings were thus determined to be 17.8 ± 1.2, 8.2 ± 0.1 and 6.7± 0.2 wt.%, respectively. The mass percentage of the TEOS coating (silica) was determined to 67 ± 0.04 wt.%. The theoretical coating fractions for the coated nanoparticles are 78 % (APTES), 78 % (MTMS), 80 % (OTES) and 68 % (TEOS) assuming that the 90 µL silanes in the reactions were completely hydrolysed and condensed on the particle surfaces. The much lower values than the theoretical values for the carbon-functional coated nanoparticles therefore suggests that a significant portion of the silanes were never properly attached to the surface of the nanoparticles and were washed away with the supernatant of the solutions used. The percentage of TEOS coating is however close to the theoretical value (68 %), and that also confirmed that the silica was completely removed from the particles by the NaOH-etching method and that TEOS was completely hydrolysed and condensed in the reaction. TEOS is known to be hydrolysed considerably faster than the carbon-functional silanes but, based on previous literature, all the silanes should have been completely hydrolysed within 180 min after mixing with the ammonia/alcohol/water suspension medium.[34, 35, 36] The results were taken as further evidence that steric effects related to the molecular configuration and conformations of the functional precursor silanes were dominant in the formation of the coatings.
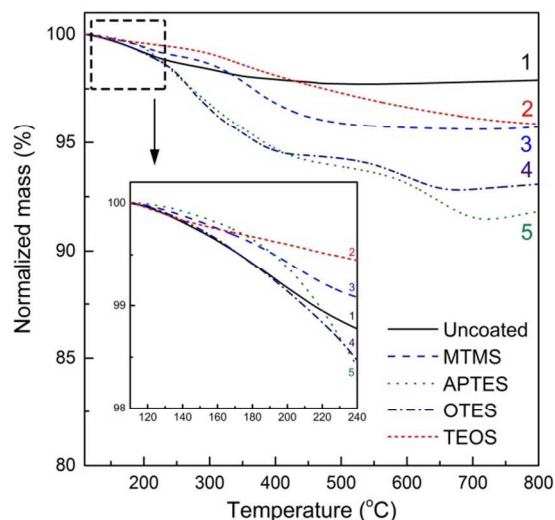


**Fig. 5.** Thermogravimetric data of synthesized core-shell nanoparticles (1) uncoated, (2) TEOS-coated (3) MTMS-coated, (4) OTES-coated, (5) APTES-coated iron oxide nanoparticles.

### 3.5 Coating densities / porosities related to the molecular structure of the silane precursors

The density of each coating was determined based on the mass fractions of the different coatings obtained by etching, and the coating volume fractions calculated from TEM imaging. Table 1 shows that all the coatings, including the TEOS-based silica coating, had very low densities.

**Table 1.** Calculated densities from coating mass measured by alkali etching, and coating volume fraction obtained from TEM data.

| Sample | Coating mass by etching (wt. %) | Coating volume by TEM (%) | Density of coating (kg·m$^{-3}$) |
|---|---|---|---|
| APTES | 17.8 | 66 | 560 |
| MTMS | 8.2 | 61 | 300 |
| OTES | 6.7 | 59 | 260 |
| TEOS | 67.0 | 92 | 920 |

The octyl-functional coating had the lowest density of all the coatings with a density of 260 kg/m$^3$, followed by the methyl-functional coating with 300 kg/m$^3$. The more hydrophilic coatings had higher densities: 560 kg/m$^3$ for the APTES- and 920 kg/m$^3$ for the TEOS-coating. It was clear not only that a long hydrophobic carbon functionality in the silsesquioxane network was detrimental for obtaining a dense coating structure but also that the small methyl unit had a pronounced negative effect on the coating density. In contrast, the APTES-coating could host a 4 times higher molar mass aminopropyl unit inside the network, while simultaneously having a density twice as high as that of the methyl-functional MTMS coatings. The fact that the TEOS-coating showed the highest density, 920 kg/m$^3$ of condensing suggests that the MTMS and OTES molecules reduce the possibility of condensing compact multi-layered silsesquioxane coatings with higher densities due to their hydrophobic nature.

The liquid densities of these coatings at 23 °C and normal pressure were calculated according to the group contribution method of van Krevelen [37]. The input data used for the calculations were taken from van Krevelen [37]. The repeating motif used was either a fully silica-like structure (the silicon atom bonded to three oxygen atoms; note that only two of them are included in the repeating unit structure) or a fully hydrolyzed structure but with no Si–O–Si bridges. The following densities were obtained: 1105 – 1134 kg m$^{-3}$ (APTES), 1180 – 1250 kg m$^{-3}$ (MTMS) and 996 – 1003 kg m$^{-3}$ (OTES). The higher values refer to the silica-like structures. The significantly lower density values presented in Table 2 thus

indicate that the coatings were porous. The porosities were calculated with reference to the liquid densities: 49 – 51 % (APTES), 75 – 76 % (MTMS) and 74 % (OTES). The density of silica-particles synthesized from TEOS using the Stöber process was 1980 kg m$^{-3}$ according to Blaaderen et al..[38] Fumed silica has a density close to 2200 kg m$^{-3}$ .[39] Hence, the porosity of the TEOS coating on the iron oxide nanoparticles was with reference to the fumed silica 58 %. Blaaderen et al.[38] reported that the density of nanoparticles prepared from a mixture of APTES/TEOS by the Stöber method was 1500 kg/m$^3$, while the density of silica particles prepared from TEOS alone was 1980 kg/m$^3$. Blaaderen et al.[38, 40] also reported that the density of the pure silica particles decreased with decreasing particle size. This decrease in density was related to a less condensed coating structure with a greater radius of curvature of the smaller sized particles.

### 3.6 Coating layers as related to the molecular conformation of the silane precursors

Fig. 6 illustrates the structures of the three silsesqiuoxane coatings and of the silica coating on the Fe$_3$O$_4$ particles. Fig. 6a shows the hydrolysed MTMS unit and an example of a possible MTMS structure with 7 layers forming a coating with a thickness of 1.8 nm as revealed by TEM. There are several important features: (i) the growth from the Fe$_3$O$_4$ surface may be partially frustrated due to the pendant methyl groups. As shown in Fig. 6a, two of the first methyl groups either terminate the growth upwards (right arrow) or adapt to an unfavourable position/orientation (left arrow). This is expected to impede the growth of the coating and to make it thinner than with TEOS and less dense than with TEOS and APTES. (ii) IR spectroscopy revealed the presence of hydroxyl groups on the coated particle surfaces. These may originate from uncoated regions on the particle and from unreacted hydroxyl groups inside and on the surface of the coating. It is shown in the MTMS coating that the uppermost surface probably contains a mixture of a Si-O-Si network, methyl groups and unreacted hydroxyl groups. However, the MTMS precursor yielded a hydrophobic coating, implying that the methyl and Si-O-Si groups dominated at the surface. Fig. 6b shows the hydrolysed TEOS monomer and a simulated TEOS silica network. It should be noted that the coating thickness indicated in Fig. 6b is for simplicity much thinner than the real thickness revealed by TEM. Compared to MTMS, it is readily seen that a more perfect network is possible with the four-armed functionality, i.e. TEOS is expected to generate a coating with a higher density.

# Journal Name

## ARTICLE
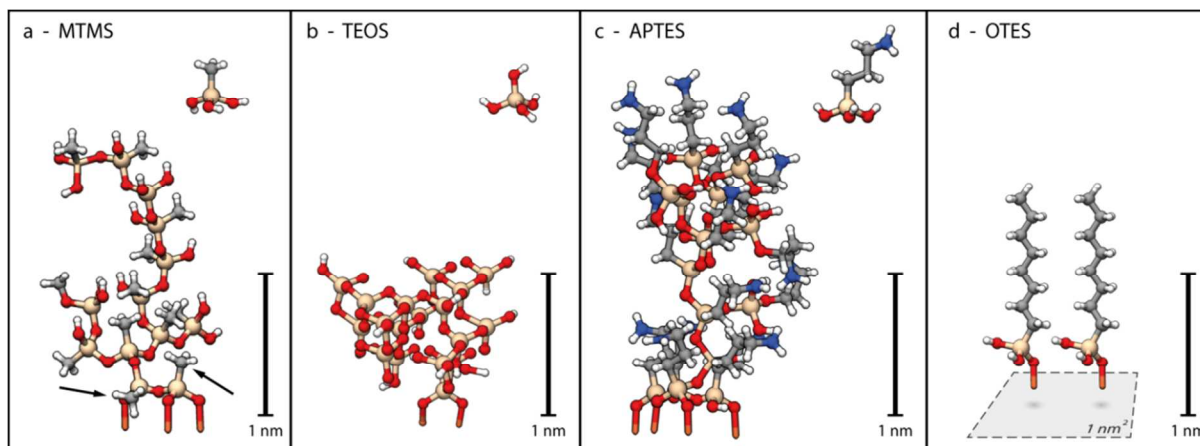


**Figure 6.** Schematic drawings of the silsesqiouxane coatings. Gold, grey, red, blue and white balls correspond respectively to Si, C, O, N and hydrogen atoms. For simplicity, the coatings are growing only from Fe atoms (orange parts of the lowermost Fe-O bonds). The structures represent monomers and coatings of a) MTMS, b) TEOS and c) APTES. Two OTES chains are displayed in d. The large and small arrows in Figure 6a refer respectively to a terminated growth in the vertical direction due to a methyl group and to a sterically unfavourable position of a methyl group.

Fig. 6c shows the hydrolysed APTES monomer and a feasible APTES coating structure. The coating consists of five layers generating a coating with a thickness of 2.1 nm as experimentally found by TEM. The fourth amine-functionalized arm also provided a more frustrated growth than TEOS. Interestingly, the amine-functional arms provided a relatively dense network with the second highest density (after TEOS), which suggested less steric repulsion during the growth of the coating layer. There must have been a tendency (based on the modelling) for the amine arms to orient upwards in a relatively extended, if the most efficient packing is considered in order to achieve the coating thickness revealed by TEM. This also means that the upper surface contains more amine than Si–O–Si and hydroxyl groups. Fig. 6d shows two OTES molecules anchored to the particle surface. The observed TEM thickness of this layer was 1.7 nm and IR revealed that there was no Si–O–Si network, (Fig. 4). The absence of a condensed silsesquioxane network meant that there could only have been two molecules per nm$^2$ at the most. In addition, the molecules have to be in an extended conformation to reach the observed coating thickness. Naik et al.[41] previously reported this model result for octadecyltrocholorosilanes. Hydroxyl groups were also present within this coating and originated from uncoated parts of the particle surface and unreacted OTES hydroxyls.

Overall it is clear that, even if these values are only rough estimates, the 5.5 nm TEOS coating where no carbon-functional units were present and the number of estimated

layers was ca. 10 matched the stoichiometric amount of TEOS precursor that was used in the reaction. It is also evident that considerable amounts of silane precursor must have been lost in the reactions with the carbon-functional precursors, due to a less efficient attachment of the silanes to the surface of the particles. The lost amounts were estimated to be: 94.2, 96.6 and 98.3 % for the APTES, MTMS and OTES, respectively.

### 3.7 ZnO and Al$_2$O$_3$ nanoparticles coated by OTES

The coating method that had been optimized for the ferrite nanoparticles was evaluated with ZnO and Al$_2$O$_3$ nanoparticles in order to verify the versatility of the reaction conditions. The OTES coating was selected for the study because it was the most challenging, both to achieve uniform and particle-covering coatings and to provide nanoparticles dispersible in hydrophobic polymers such as polyethylene. Figs. 7a and b show transmission electron micrographs of pristine and coated ZnO particles. The ZnO particles (average size = 25 nm) showed dominantly well-developed coatings, although the larger particles showed a somewhat less pronounced core-shell structure. The coating thickness was approximately 2 nm. The method was also applicable to the spherical Al$_2$O$_3$ nanoparticles (average size = 45 nm; Fig. 8c); the coating thickness in this case was also ca. 2 nm (Fig. 8d). The coating thickness was essentially uniform, i.e. independent of the nanoparticle size (Fig. 8d).

# Journal Name

## ARTICLE
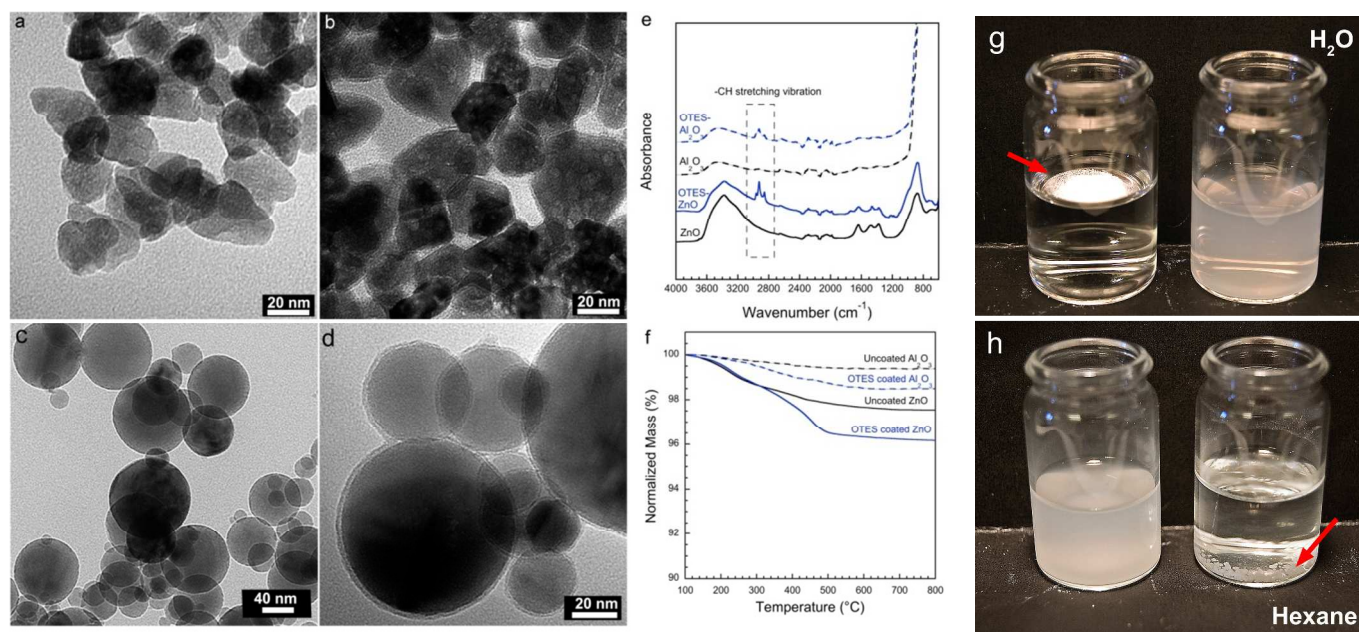


**Fig. 7.** TEM of (a) uncoated ZnO, (b) OTES coated ZnO, (c) uncoated $Al_2O_3$, (d) OTES coated $Al_2O_3$, (e) IR spectra of uncoated and coated ZnO and $Al_2O_3$ NPs, (f) TG data of uncoated and coated ZnO and $Al_2O_3$ NPs. (g) OTES coated $Al_2O_3$ on water (left) and uncoated $Al_2O_3$ in water (right), (h) OTES coated $Al_2O_3$ in hexane (left) and uncoated $Al_2O_3$ sedimented in hexane (right).

The clearer core-shell structure for the coated $Al_2O_3$ nanoparticles made possible an accurate assessment of the volume fraction of the coating, $22.5 \pm 5$ vol.% which, assuming that the coating density was 260 kg/m$^3$, corresponds to a mass fraction of $1.8 \pm 0.4$ %. The mass loss of the coated $Al_2O_3$ nanoparticles at 800 °C relative to that of the uncoated $Al_2O_3$ nanoparticles was ca. 0.88 wt.% (Fig. 7f). This corresponds to an approximate coating fraction of ca. 1.4 wt.%, which was in agreement with the predication based on TEM. The OTES-coated ZnO nanoparticles showed a mass loss of 1.4 % at 800 °C relative to that of the pristine nanoparticles, suggesting a coating fraction of ca. 2.2 wt.%.

The IR spectra displayed in Fig. 7e confirmed the presence of the coatings on the nanoparticles through the absorption bands assigned to the C–H stretching vibration at 2800–2950 cm$^{-1}$, the –CH$_2$ bending vibration at 1450 and 1374 cm$^{-1}$ and the Si–C stretching vibration at 1213 cm$^{-1}$. The absence of the Si–O–Si stretching vibration band appearing between 800 and 1100 cm$^{-1}$ also confirmed that the silica network formation was impeded by the carbon functionality of OTES as in the case of the ferrite nanoparticles. Fig. 7g shows the OTES coated $Al_2O_3$ nanoparticles solubility in water (top) and in hexane (bottom) as compared to uncoated $Al_2O_3$ nanoparticles. The effectively applied octyl-functional silsesquioxane coating renders the

particle completely immiscible with the water and miscible with the hydrocarbon-based hexane, respectively.

## 4. Conclusions

It is here demonstrated that relatively thick and uniform silsesquioxane coatings can be applied to different inorganic nanoparticles cores in single-step reactions with three different types of carbon-functional silanes (methyl-, octyl-, and aminopropyl-functional). The coatings were evaluated on 8 nm $Fe_3O_4$, 25 nm ZnO and 45 nm $Al_2O_3$ – without the use of surfactants or capping agents, and represented ca. 60–70 vol.% of the prepared core-shell iron oxide nanoparticles. The larger octyl-functional silsesquioxane precursor showed the thinnest coatings with the lowest coating density of 260 kg/m$^3$, followed by the methyl functional coating at 300 kg/m$^3$. Atomistic modelling showed that the growths of both this coating and that of the methyl-functional coating were frustrated. Accordingly, the low densities originated from the methyl and the octyl groups introduced steric hindrance, resulting in only a few growing molecules per unit area, the growth stopping at a certain coating thickness and the formation of the cross–linked silicon oxide structure being hindered. The octyl-functional silsesquioxane coatings showed no sign of Si–O–Si absorption according to IR spectroscopy for the three core particles studied, even though the coatings were readily visible in TEM

micrographs. The more hydrophilic amino-functional coating and the silica coating showed higher densities, 560 and 920 kg/m$^3$ respectively. The high density of the latter coatings was due to the formation of a more densely cross-linked silicone oxide network on the nanoparticles, which was confirmed by IR spectroscopy, and their ability to pack more efficiently due to their strongly hydrophilic character. The densities of the coatings were determined gravimetrically on the powder samples before and after alkaline etching, which proved to be a more accurate method of determining the coating fraction than relying on calculated coating percentages based on thermogravimetric data. The developed coating chemistry has the potential to be used as bridging chemistry for further nanoparticle modification, e.g. atomic radical polymerisation from amino-functional particle surfaces.

## Acknowledgements

## Notes and references

$^a$ KTH-Royal Institute of Technology, School of Chemical Science and Engineering, Fibre and Polymer Technology SE-100 44 Stockholm, Sweden

* Corresponding author E-mail: rols@kth.se

Electronic Supplementary Information (ESI): Dynamic Light Scattering (DLS) data and electron micrographs. See DOI: 10.1039/b000000x/

1.  T. Hjertberg, V. Englund, P. O. Hagstrand, W. Loyens, U. Nilsson and A. Smedberg, In Proc. Jicable-HVDC'2013, France, 2013, p 2.1.
2.  M. Jeroense, M. Saltzer and H. Ghorbani, In Proc. Jicable-HVDC'13, France, 2013, p 1.1.
3.  A. Gustafsson, M. Saltzer, A. Farkas, G. Ghorbani, T. Quist and M. Jeroense, Technical Paper ABB Grid System, 2014.
4.  The Megavolt challenge A strategic Research and Innovation Agenda, Elforsk AB, Stockholm, 2014.
5.  S. Gubanski and U. Gedde, In Proc. Jicable-HVDC'13, France, 2013, p 3.2.
6.  M. Iijima, M. Kobayakawa, M. Yamazaki, Y. Ohta and H. Kamiya, *J. Am. Chem. Soc.*, 2009, 131, 16342.
7.  S. Ding, Y. Xing, M. Radosz and Y. Shen, *Macromolecules*, 2006, 39, 6399.
8.  S. Kango, S. Kalia, A. Celli, J. Njuguna, Y. Habibi and R. Kumar, *Prog. Polym. Sci.*, 2013, 38, 1232.
9.  A.-L. Morel, S. I. Nikitenko, K. Gionnet, A. Wattiaux, J. Lai-Kee-Him, C. Labrugere, B. Chevalier, G. Deleris, C. Petibois and A. Brisson, *Acs Nano*, 2008, 2, 847.
10. X. Zhang, S. Mansouri, L. Clime, H. Ly, L. H. Yahia and T. Veres, *J. Mater. Chem.*, 2012, 22, 14450.
11. Y. Han, J. Jiang, S. S. Lee and J. Y. Ying, *Langmuir*, 2008, 24, 5842.
12. A. Goyal, A. Kumar and P. M. Ajayan, *Chem. Commun.*, 2010, 46, 964.
13. X. Huang, A. Schmucker, J. Dyke, S. M. Hall, J. Retrum, B. Stein, N. Remmes, D. V. Baxter, B. Dragnea and L. M. Bronstein, *J. Mater. Chem.*, 2009, 19, 4231.
14. L. M. Liz-Marzán, M. Giersig and P. Mulvaney, *Langmuir*, 1996, 12, 4329.
15. R. T. Olsson, M. S. Hedenqvist, V. Ström, J. Deng, S. Savage and U. W. Gedde, *Polym. Eng. Sci.*, 2011, 51, 862.
16. W. Stöber, A. Fink and E. Bohn, *J. Colloid Interface Sci.*, 1968, 26, 62.
17. C. Graf, D. L. Vossen, A. Imhof and A. van Blaaderen, *Langmuir*, 2003, 19, 6693.
18. A. Guerrero-Martínez, J. Pérez-Juste and L. M. Liz-Marzán, *Adv. Mater.*, 2010, 22, 1182.
19. J. Yang, D. Shen, L. Zhou, W. Li, X. Li, C. Yao, R. Wang, A. M. El-Toni, F. Zhang and D. Zhao, *Chem. Mater.*, 2013, 25, 3030.
20. E. von Haartman, H. Jiang, A. A. Khomich, J. Zhang, S. A. Burikov, T. A. Dolenko, J. Ruokolainen, H. Gu, O. A. Shenderova and I. I. Vlasov, *J. Mater. Chem. B*, 2013, 1, 2358.
21. Y. Zhang, X. Kong, B. Xue, Q. Zeng, X. Liu, L. Tu, K. Liu and H. Zhang, *J. Mater. Chem. C*, 2013, 1, 6355.
22. C. Wu, Z.-Y. Lim, C. Zhou, W. G. Wang, S. Zhou, H. Yin and Y. Zhu, *Chem. Commun.*, 2013, 49, 3215.
23. V. Strom, R. T. Olsson and K. V. Rao, *J. Mater. Chem.*, 2010, 20, 4168.
24. M. Fang, V. Ström, R. T. Olsson, L. Belova and K. V. Rao, *Nanotechnology*, 2012, 23, 145601.
25. M. Fang, V. Ström, R. T. Olsson, L. Belova and K. V. Rao, *Appl. Phys. Lett.*, 2011, 99, 222501.
26. A. M. Pourrahimi, D. Liu, L. K. H. Pallon, R. L. Andersson, A. Martinez Abad, J. M. Lagaron, M. S. Hedenqvist, V. Strom, U. W. Gedde and R. T. Olsson, *RSC Adv.*, 2014, 4, 35568.
27. Y. Lu, Y. Yin, B. T. Mayers and Y. Xia, *Nano Lett.*, 2002, 2, 183.
28. X. Yang, N. Zhao, Q. Zhou, C. Cai, X. Zhang and J. Xu, *J. Mater. Chem. C*, 2013, 1, 3359.
29. S. Roy, C. K. Dixit, R. Woolley, B. D. MacCraith, R. O'Kennedy and C. McDonagh, *Langmuir*, 2010, 26, 18125.
30. H. G. Pryce Lewis, D. J. Edell and K. K. Gleason, *Chem. Mater.*, 2000, 12, 3488.
31. J. Feng, G. H. Xu, Y. An and X. Zeng, *Colloids Surf., A*, 2008, 316, 194.
32. J. Azadmanjiri, G. P. Simon, K. Suzuki, C. Selomulya and J. D. Cashion, *J. Mater. Chem.*, 2012, 22, 617.
33. J. Lin, J. A. Siddiqui and R. M. Ottenbrite, *Polym. Adv. Technol.*, 2001, 12, 285.
34. H. Jiang, Z. Zheng, Z. Li and X. Wang, *Ind. Eng. Chem. Res.*, 2006, 45, 8617.
35. Y. Liu, Y. Li, X.-M. Li and T. He, *Langmuir*, 2013, 29, 15275.
36. C. J. Brinker, *J. Non-Cryst. Solids*, 1988, 100, 31.
37. X. van Krevelen. Properties of polymers, 3$^{rd}$ Edition, Amsterdam: Elsevier, 1990, pp. 71–83.
38. A. van Blaaderen and A. Vrij, *J. Colloid Interface Sci.*, 1993, 156, 1.
39. A. Van Blaaderen and A. Kentgens, *J. Non-Cryst. Solids*, 1992, 149, 161.
40. I. K. Ralph. The chemistry of silica, John Wiley & Sons, Inc., United States, 1979, pp. 3–29.
41. V. V. Naik, M. Crobu, N. V. Venkataraman and N. D. Spencer, J. Phys. Chem. Lett. 2013, 4 (16), 2745.